Int. J. Heat Mass Transfer. Vol. 21, pp. 1175–1184

0017-9310/78/0901-1175 $02.00/0

IMPINGEMENT OF AN AXISYMMETRIC LIQUID JET ON A BARRIER

V. E. NAKORYAKOV, B. G. POKUSAEV and E. N. TROYAN
Institute of Thermophysics, Siberian Branch of the USSR Academy of Sciences, Novosibirsk, USSR

(*Received* 9 *September* 1976 *and in revised form* 8 *July* 1977)

Abstract—In some metallurgical and chemical engineering technologies utilization of heavy liquid jets impinging onto a wall appears to be an effective tool for the enhancement of heat- and mass-transfer processes. The aim of the present work was to study, both theoretically and experimentally, hydrodynamics and mass transfer of a radial liquid jet impinging onto a horizontal plane. The whole field of the flow—from the stagnation point to the hydraulic jump—is described within the scope of approximations of the boundary-layer theory for both laminar and turbulent regimes of flow in a thin liquid layer. Simple formulas have been obtained for calculation of the friction factor, liquid layer thickness and the liquid surface velocity as a function of discharge parameters. Solution has been offered to the problem of mass transfer from the wall to a liquid layer for the whole laminar flow region upstream of the jump and simple working formulas have been obtained for calculation of the mass-transfer coefficient. Wall shear stresses, local and mean mass-transfer coefficients within the entire flow region have been measured by an electrodiffusion method in a wide range of liquid flow rates and the conditions at which the flow leaves the barrier. Hydrodynamic characteristics of the jet at the location of impact and of the hydraulic jump have also been studied. The experimental results are given in terms of generalized coordinates and compared with the appropriate theoretical equations.

NOMENCLATURE

Re, Reynolds number;
Pr, diffusional Prandtl number;
D, diffusion coefficient [m^2/s];
Nu, diffusional Nusselt number;
C_f, friction factor;
Q, volumetric liquid flow rate [m^3/s];
C, concentration [g-eq/m^3];
q, mass flux density [g-eq/m^2 s];
F, Faraday number [C/g-eq];
g, gravitational acceleration [m/s^2];
S, probe surface area [m^2];
W, velocity of disturbance propagation on shallow water [m/s];
H, nozzle-to-plate spacing [m];
L, rim height above disk [m];
A, nozzle diameter [m];
U, liquid surface velocity [m/s];
d, probe diameter [m];
h, liquid film thickness [m];
l, linear dimension [m];
a, constant in formula (1);
t, temperature [°C];
x, y, r, z, coordinates;
u, ω, velocity components.

Greek symbols

τ, shear stress [N/m^2];
ν, kinematic viscosity [m^2/s];
μ, dynamic viscosity [$N \cdot s/m^2$];
ρ, density [kg/m^3];
δ, boundary-layer thickness [m];
β, mass-transfer coefficient [m/s];
ω, axial velocity [m/s];
σ, surface tension [N/m].

Subscripts

+, section in which a boundary layer converges with liquid film thickness;
0, minimal jet cross-section area;
I, hydraulic jump cross-section area;
f, value at wall;
∞, value at infinity;
d, diffusional.

Superscript

′, pulsation value.

1. INTRODUCTION

WHEN liquid jets impinge on a barrier (Fig. 1), the liquid spreads over the surface as a thin layer bounded by a hydraulic jump beyond which the depth of the liquid is much greater. In Fig. 1, r and z are the longitudinal and transverse coordinates, r_0 is the radius of the minimal jet cross-section area. The whole field of the flow may conventionally be divided into the potential (I) and viscous (II) regions. The potential region may, in turn, be subdivided into:

1. The region of a free impinging jet;
2. The region of jet deflection;
3. The region of a free radial jet.

The viscous flow region may be subdivided into [1]:

1. The region of the forward stagnation point whose dimensions are of the order of the jet radius r_0. Within this region the main flow velocity, u, grows rapidly from zero to the undisturbed flow velocity U_0;
2. The region of the boundary-layer type flow at $r > r_0$, where a streamwise pressure gradient is practically absent and the velocity outside the boundary layer is constant and equal to U_0;

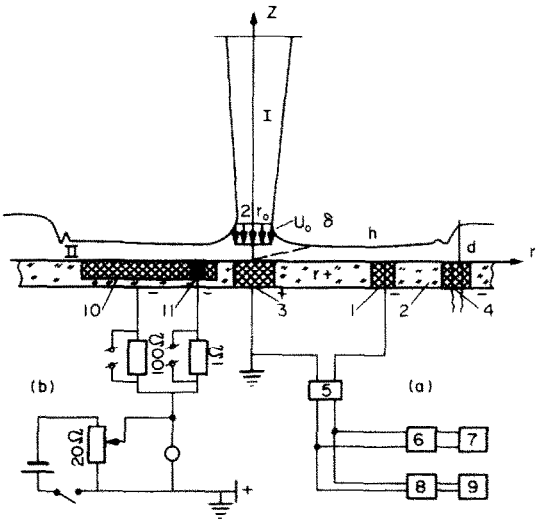

FIG. 1. Near-barrier liquid flow pattern and scheme for friction and mass transfer coefficient measurements: 1, friction probe; 2, disk; 3, anode; 4, double probe; 5, constant current amplifier; 6, filter; 7,8, potentiometers; 9, squaring arrangement.

3. The region of transition where the boundary layer becomes as thick as the liquid film at $r \approx r_+$;

4. The region having a similarity velocity profile. Below, this region will be referred to as the flow downstream of the convergence point or as the region of "hydrodynamic stabilization";

5. The region of the hydraulic jump;

6. The region of undisturbed flow downstream from the hydraulic jump.

The spatial flow in the vicinity of the stagnation point is one of the problems having an exact solution of the Navier–Stokes equations. This problem was solved by Schlichting [2], who found that in the neighborhood of the forward stagnation point the shear stress is defined as

$$\tau = 1.312 \cdot \rho a (a \cdot \nu)^{1/2}, \qquad (1)$$

where, according to [3],

$$a = 0.44 U_0 / r_0.$$

The most complete theoretical analysis of the axisymmetric and two-dimensional impinging jets is given by Watson in [1]. His analysis involves the solution of the following problems:

(a) Laminar boundary layer-type flow. Here, the Blasius profile for a plate is used and the friction factor is found from

$$C_f/2 = 0.575 \cdot (\nu / U_0 \cdot r)^{1/2}. \qquad (2)$$

(b) Downstream of the point of boundary-layer convergence with the film surface ($r > r_+$), the surface velocity of the film and its thickness are determined.

(c) In the transition region, the velocity profile changes its shape from the Blasius type to the similarity one, however, both not very much differing from each other [1]. In this case, at $r_0 \ll r < r_+$, the boundary-layer thickness $\delta < h$ and $U = U_0$, while in the steady-state flow region, where $r > r_+$, $U < U_0$ and $\delta = h$.

(d) The turbulent flow is calculated with the help of the eddy viscosity, in the form proposed by Glauert [4], and the Blasius law for friction at the wall.

The boundary-layer-type flow problem is solved by the method of integral equations.

The heat-transfer problem of an axisymmetric impinging liquid jet was solved by Chaudhury [5] based on the entire flow division into the regions which had been adopted in [1].

An experimental check of the normal liquid jet pressure distribution on the surface, calculated in [6] as a function of the jet incidence angle, was undertaken by Grigoryan in [7], who found a 3%-discrepancy between the experiment and prediction by the momentum equation.

A most complete investigation of the hydrodynamics of a viscous fluid layer, being formed by an axisymmetric jet impinging onto a plate, was made by Olsson [8] for a wide range of flow rates and viscosities. His measurements of the liquid film thickness, the layer kinematic energy prior to a hydraulic jump as a function of the radius and the layer surface velocity show that:

1. The thickness of the liquid layer downstream of the jump is an order above that upstream and hardly varies along the plate radius.

2. Data on the layer thickness in the jump zone are at an essential variance with predicted values for inviscid fluid ($h = r_0^2/2r$) much over the entire flow region.

3. The layer surface velocity remains constant up to the jump, i.e. the boundary layer emerges onto the surface at greater values of r, than it was predicted by Watson [1].

Rao and Olev [9] investigated mass transfer from a horizontal plate, covered with a layer of transcinnamic acid, to a vertical turbulent submerged water jet falling into the plate center. All the experiments were carried out at $t = 25°C$ within the range of the Reynolds numbers $Re = U_0 A/\nu = (25\text{–}125) \cdot 10^3$ at $Pr = 900$. The experimental data for $x/A < 4.5$, where x is the distance from the plate center, A the nozzle diameter, are given in empirical equations. For $H/A < 6.5$, the mean Nusselt number in the impact region is given by

$$\beta \cdot A/D = 0.046 \cdot Re^{1.06} (H/A)^{-0.09} \qquad (3)$$

and for $H/A \geq 6.5$ it is given by

$$\beta \cdot A/D = 0.107 \cdot Re^{1.06} (H/A)^{-0.54}, \qquad (4)$$

where β is the mean mass-transfer coefficient.

With $x/A > 4.5$, there is a power-law dependence between the local Nu number and x/A, with $Nu = f(x/A)$ being independent of H/A

$$Nu = \beta A/D = 1.3 (A \cdot U \cdot \rho/\mu)^{0.84} (x/A)^{-1.27} \qquad (5)$$

The experiments on heat transfer between a two-dimensional liquid jet and a heated plate [10] show that in the neighborhood of the jet impingement the measured heat-transfer coefficients (at the wall temperature T being less than the saturation temperature T_s)

Table 1.

Flow region	Laminar flow	Nos.	Turbulent flow	Nos.
II-1	$\frac{\tau \cdot Q^2}{\rho \cdot \nu^4} = 5.95 \times 10^{-2}(Q/\nu r)^{7/2} \cdot (r/r_0)^{9/2}$ the Schlichting–Shach formula	(1a)	$C_f/2 = (Q \cdot 0.435/\pi^{1.5})(\nu/U_0 \cdot r)^{1/5}$ or	(16)
	$C_f/2 = 0.577(\nu/U_0 \cdot r)^{1/2}$ or	(11)	$\frac{\tau Q^2}{\rho \nu^4} = \frac{0.0435}{\pi^2}(Q/\nu r)^{1/5}(Q/\nu r_0)^{18/5}$	(17)
II-2	$\frac{\tau Q^2}{\rho \nu^4} = 0.104\left(\frac{Q}{\nu r}\right)^{1/2} \cdot \left(\frac{Q}{\nu r_0}\right)^3$	(12)		
	$r_+ = 0.257 \cdot r_0(Q/\nu r_0)^{1/3}$	(13)	$r_+ = 1.62 \cdot r_0(Q/\nu r_0)^{1/9}$	(18)
II-4	$\frac{\tau \cdot Q^2}{\rho \cdot \nu^4} = \frac{(10\pi/9)(Q/\nu r)^3}{[(10\pi/9)(Q/\nu r)^{-1} + (r_0/r)^2 0.476]^2}$ at $r \gg \nu_+$	(14)	$\frac{\tau Q^2}{\rho \nu^4} = \frac{2.9(Q/\nu r)^{15/4}}{[(Q/\nu r)^{-1/4} + 24(r_0/r)^2]^2}$ at $r \gg r_+$	(19)
	$\frac{\tau Q^2}{\rho \nu^4} = 3.9 \times 10^{-2}(Q/\nu r)^5$	(15)	$\frac{\tau Q^2}{\rho \nu^4} = 2.9(Q/\nu r)^{17/4}$	(20)

are correlated by

$$Nu_x = 0.73 Pr^{1/3}(kRe_x)^{0.5}, \quad (6)$$

$$Nu_x = 0.037 Pr^{1/3}(kRe_x)^{0.8} \quad (7)$$

for the laminar (6) and turbulent (7) boundary layers, respectively. According to [11], relationships (6) and (7) differ from analogous relations for a uniform parallel flow since heat transfer is essentially affected by the hydrodynamic characteristics of the jet (velocity and pulsation distribution near the stagnation point), which are accounted for in (6) and (7) by the correction factor k.

As seen from the above analysis, in the pertinent literature there are neither analytical formulae for calculation of the local and mean mass-transfer coefficients, nor any simple (engineering) method for calculating the friction as a function of the jet discharge parameters in all the flow regions in laminar and turbulent regimes. To the best of the authors' knowledge, reported experimental data on mass transfer are scanty [9] and the data on friction factors are not available at all. These have become the objects of the present investigation.

2. CALCULATION OF WALL FRICTION FOR LIQUID JET IMPINGEMENT ON THE WALL

Below we give the results of calculations for the laminar and turbulent film flows in the II-2 and II-4 regions, which have been aimed at deriving simple formulae for the friction factors and dimensionless parameters to correlate the experimental results. The calculation is carried out within the scope of the boundary-layer approximations by the Shvets method [11] (the method of successive approximations) distinguished for its simplicity in regard to the present problem.

For a laminar flow, the starting system of equations and the boundary conditions are of the form [1, 12]:

$$u\frac{\partial u}{\partial r} + \omega\frac{\partial u}{\partial z} = \nu\frac{\partial^2 u}{\partial z^2}, \qquad \frac{\partial(ru)}{\partial r} + \frac{\partial r(\omega)}{\partial z} = 0 \quad (8)$$

$$\left.\begin{array}{ll} u = \omega = 0 & \text{at } z = 0 \\ u = U_0; \partial u/\partial z = 0 & \text{at } z = \delta \end{array}\right\} \text{for the II-2 region} \quad (9)$$

$$\left.\begin{array}{ll} u = \omega = 0 & \text{at } z = 0 \\ \partial u/\partial z = 0 & \text{at } z = h \end{array}\right\} \text{for the II-4 region.} \quad (10)$$

For a turbulent flow, the problem is solved by the use of the Blasius law for friction and the power-law velocity distribution $u = (z/\delta)^{1/7} \cdot U_0$.

A detailed solution of the problem is given elsewhere [12], therefore here only the main formulae are presented (see Table 1).

Comparison with the analysis performed by Watson shows that formulae (11), (14), (16), (19) virtually coincide with the corresponding formulae suggested by Watson [1]. It is also evident that the experimental results can be given in terms of the generalized coordinates $[\tau Q^2/r\nu^4;\ Q/\nu r]$, therefore below the experimental data will be compared with formulae (11)–(20).

3. CALCULATION OF MASS TRANSFER OF AN IMPINGING RADIAL LIQUID JET

3.1. *Laminar regime in the boundary-layer-type flow region*

Near the streamlining surface the following is valid:

$$u = \left(\frac{\partial u}{\partial z}\right)_{z=0} \cdot z.$$

Then the solution of the hydrodynamic problem yields:

$$u = \left(\frac{U_0}{\delta} + \frac{U_0^2}{24\nu} \cdot \frac{d\delta}{dr} + \frac{U_0^2}{24\nu} \cdot \frac{\delta}{r}\right) z. \quad (21)$$

Substituting $\delta = 2.32(\nu r/U_0)^{1/2}$ into (21) gives

$$u = 1.34 z U_0/\delta, \tag{22}$$

then from (8)

$$\omega = -\frac{1.34}{4}\cdot\frac{U_0\cdot z^2}{\delta r}. \tag{23}$$

The diffusion equation is of the form

$$u\frac{\partial c}{\partial r} + \omega\frac{\partial c}{\partial z} = D\cdot\frac{\partial^2 c}{\partial z^2} \tag{24}$$

with the boundary conditions

$$C(z=0;r)=0;\quad C(z=\infty;r)=C_\infty. \tag{25}$$

Here C is the concentration of the oxidized ions and C_∞ is the concentration of ions far from the wall.

Substitute velocity distributions (22) and (23) into (24)

$$\frac{\partial^2 C}{\partial z^2} + \frac{A}{D\cdot 4}\cdot\frac{z}{r}\cdot\frac{\partial C}{\partial z} = \frac{A}{D}\cdot z\cdot\frac{\partial C}{\partial r}, \tag{26}$$

where $A = 1.34\cdot U_0/\delta$.

Next, introduce a new independent variable [13], $\eta = \frac{1}{2}(U_0/\nu r)^{1/2}\cdot z$. Then equation (26) transforms into an ordinary differential equation

$$\frac{\mathrm{d}^2 C}{\mathrm{d}\eta^2} + aPr\cdot\eta^2\frac{\mathrm{d}C}{\mathrm{d}\eta} = 0;\quad a = 3.46, \tag{27}$$

with the boundary conditions $C(0)=0$ and $C(\infty)=C_\infty$. Integrating (27) yields

$$C = C_\infty\int_0^\eta \exp\left(-\frac{a}{3}Pr\cdot\eta^3\right)\mathrm{d}\eta \Big/ \int_0^\infty \exp\left(-\frac{a}{3}Pr\cdot\eta^3\right)\mathrm{d}\eta. \tag{28}$$

The integral in (28) is expressed via the gamma-function to give

$$\int_0^\infty \exp\left(-\frac{a}{3}Pr\cdot\eta^3\right)\mathrm{d}\eta = 0.897\Big/\left(\frac{a}{3}Pr\right)^{1/3}$$

and finally

$$C = \frac{(a/3\cdot Pr)^{1/3}\cdot C_\infty}{0.897}\int_0^\eta \exp\left(-\frac{a}{3}Pr\cdot\eta^3\right)\mathrm{d}\eta. \tag{29}$$

Now, when the concentration distribution (29) is known, we can define the diffusional flux directed to the plate

$$q = 0.59 D\cdot C_\infty\ Pr^{1/3}(U_0/\nu r)^{1/2}. \tag{30}$$

In a dimensionless form the latter expression is reduced to

$$Nu = 0.59\cdot Pr^{1/3}\cdot Re_r^{1/2} \tag{31}$$

or

$$\frac{\beta Q}{D^2} = \frac{0.59}{\pi^{1/2}}\cdot Pr^{4/3}\left(\frac{Q}{\nu r}\right)^{3/2}\cdot\left(\frac{r}{r_0}\right). \tag{32}$$

The diffusional layer thickness may be evaluated as

$$\delta_d = 1.7\cdot Pr^{-1/3}\cdot Re^{-1/2}. \tag{33}$$

3.2. *Laminar flow downstream of the convergence point*

Assuming that $u = (\partial u/\partial z)_{z=0}\cdot z$ is valid near the surface, we receive from the solution of the hydrodynamic problem that

$$u = \frac{Q^2}{3\nu\pi^2}\left(\frac{1}{r^3 h} + \frac{1}{r^2 h^2}\cdot\frac{\partial h}{\partial r}\right)z. \tag{34}$$

$$h = h_+\cdot\frac{r_+}{r} + \pi\cdot\frac{10}{9}\left(\frac{\nu r}{Q}\right)\left(r^3 - r_+^3\right). \tag{35}$$

We shall seek the solution at $(r/r_+)\gg 1$, then from (35) $h \approx (10/9)\pi(\nu r^2/Q)$ and the longitudinal velocity $u = (B/r^5)\cdot z$. From continuity equation (8)

$$\omega = \frac{2B}{r^6}\cdot z^2,\quad \text{where}\quad B = \frac{9}{10}\frac{Q^3}{\nu^2\pi^3}.$$

Substitute the velocity profiles into the diffusion equation (24) with the boundary conditions $C(z=0;r)=0$, $C(z=\infty;r)=C_\infty$.

$$\frac{\partial^2 C}{\partial z^2} - \frac{2B}{D\cdot r^6}\cdot z^2\frac{\partial C}{\partial z} = \frac{A}{D\cdot r^5}\cdot z\cdot\frac{\partial C}{\partial r}. \tag{36}$$

Introduce a new independent variable

$$\eta = z\left[r^6\int_r^\infty \frac{D}{B}\cdot\frac{1}{r}\cdot\mathrm{d}r\right]^{-1/3} = \left(\frac{9}{10}\right)^{1/3}\cdot\frac{Q}{\pi\cdot\nu^{2/3}\cdot D^{1/3}\cdot r^2\ln r/r_+}. \tag{37}$$

Then equation (36) transforms into an ordinary differential equation

$$\frac{\mathrm{d}^2 C}{\mathrm{d}\eta^2} + \tfrac{1}{3}\eta^2\cdot\frac{\mathrm{d}C}{\mathrm{d}\eta} = 0. \tag{38}$$

The solution of equation (38) is of the form

$$C = C_\infty\int_0^\eta \exp(-\tfrac{1}{9}\eta^3)\mathrm{d}\eta \Big/ \int_0^\infty \exp(-\tfrac{1}{9}\eta^3)\mathrm{d}\eta. \tag{39}$$

Then the mass flux in the hydrodynamic steady-state region is defined by

$$q = D\rho\left(\frac{\partial C}{\partial z}\right)_{z=0} = \frac{DC_\infty}{\int_0^\infty \exp(-\frac{1}{9}\eta^3)\mathrm{d}\eta}\left(\frac{\partial\eta}{\partial z}\right)_{z=0} = \left(\frac{9}{10}\right)^{1/3}\frac{1}{1.86}\cdot\frac{D^{2/3}\cdot C_\infty\cdot Q}{\nu^{2/3}\cdot r^2\cdot\ln r/r_+}. \tag{40}$$

In the dimensionless form

$$Nu = \frac{\beta\cdot r}{D} = \frac{(0.9)^{1/3}}{1.86\pi}\left(\frac{Q}{\nu r}\right)\cdot Pr^{1/3}\cdot\frac{1}{\ln r/r_+}, \tag{41}$$

or

$$\frac{\beta Q}{D^2} = \frac{(0.9)^{1/3}}{1.86\pi}\cdot Pr^{4/3}\left(\frac{Q}{\nu r}\right)^2\cdot\frac{1}{\ln r/r_+}. \tag{42}$$

4. EXPERIMENTAL STUDY OF THE WALL SHEAR STRESS

4.1. *Experimental procedure and facility*

The basic technique used for measurement of the wall friction, when liquid film spreads radially over it, is the electrodiffusion method. The measurements are made in all flow regions.

The electrodiffusion method has long been known and described in detail elsewhere [12, 14–17]. We recall only that the method consists essentially of measuring the limited diffusion current J in an electrochemical cell which consists of: probe-electrode (1) with a small surface, imbedded flush with wall (2); anode (3) with a large surface; a working liquid, electrolyte, which was an equimolar ferri–ferrocyanide solution in a 0.5 normal alkali solution (NaOH) (Fig. 1).

The mass flux per unit electrode surface is related to the current J as

$$q = J/F \cdot z \cdot S, \tag{43}$$

where z is the amount of transported electrones, here $z = 1$, F is the Faraday number and S is the cathode area.

To calculate friction in the neighborhood of this point, the jet velocity and its radius in the minimal cross-section are to be known.

The jet velocity U_0 was measured by an electrodiffusion anemometer of the "forward stagnation point"-type, for which the following relation is known [14]

$$Nu = 0.753 Pr^{1/3} \cdot Re^{1/2}, \tag{46}$$

where Nu and Re are based on the liquid velocity in the jet and the radius of the outer envelope of the probe. Then, knowing the limiting diffusion current, the flow velocity can be readily calculated from (46). The minimal jet radius was determined by the optical method. The measured values of r_0 and U_0 for all the liquid flow rates are listed in Table 2.

Table 2.

No.	1	2	3	4	5	6	7	8	9	10	11	12	13	14
$Q \cdot 10^5$ m^3/s	1.36	1.88	2.64	3.80	6.9	12.1	14.0	15.7	17.3	18.83	22.4	24.3	28.3	32.0
r_0 mm	1.7	2.0	2.35	2.8	3.8	4.38	4.44	4.51	4.57	4.58	4.66	4.73	4.90	4.95
U_0 m/s	1.49	1.5	1.52	1.55	1.53	2.01	2.25	2.46	2.63	2.84	3.26	3.46	3.78	4.15

The formula for calculation of the wall shear stress in the case of an l-long plane probe of the width b, located streamwise, is of the form

$$\tau = 1.87 \mu J^3 / F^3 D^2 l^2 b^3 C_\infty^3, \tag{44}$$

while for a circular probe of the diameter d it is

$$\tau = 3.16 \mu J^3 / F^3 d^5 C_\infty^3 D^2. \tag{45}$$

A liquid jet discharges freely from a 10 mm dia nozzle orifice onto a horizontal barrier which is a 420 mm dia disk separated by 100 mm from the nozzle outlet in all the tests. The resistance of the liquid, running down from the disk, varied depending on the shape of the disk edge: rounded, sharp and the one elevated over the disk surface by 0.5; 1 and 2 mm. Probes 1 and 4 (Fig. 1) (platinum plates 0.05 mm long and 0.6 mm wide) as well as large-surface anode 3 were imbedded flush with the disk surface to measure friction. Here, to measure the main mass-transfer coefficient, probe 10 is also placed which is a 20 mm wide and 200 mm long nickel plate, in turn involving 2 mm dia nickel wires (probes 11) to measure the local mass-transfer coefficients.

The electric circuits for measuring the mean and pulsation friction as well as the local and mean mass-transfer coefficients are shown in Figs. 1(a) and 1(b), respectively. The limiting diffusion current in the circuit of the mean and local mass-transfer probes is determined by the voltage drop in the 100 Ω and 1 Ω precision resistors. The results of measurements of the mass-transfer coefficients were verified by comparing with the mean mass transfer from the plate and the readings of the local probes.

The friction probes were calibrated near the stagnation point where the dependence (1) of the shear stress on the jet liquid flow rate is known.

Besides, with the help of an electrocontact method, measurements were made of the liquid film thickness in the region of the hydraulic jump. With the use of the calibrated friction probes, the errors in the measured τ and the mass-transfer coefficients did not exceed 7 and 3.5%, respectively.

4.2. *Mean friction measurements*

The measured data on mean friction at the disk with a rounded edge were first reported in [12, 15].

Figure 2 presents characteristic results of the measurement of friction at the disk for all the flow regions, including that of a hydrodynamic jump, for the same liquid flow rate but different shapes of the disk edge. The curves show that at the point of jet impingement, when a radial velocity outside the boundary layer increases rapidly from zero at the stagnation point to U_0, the shear stress grows linearly with the radius and achieves the maximum value at r/r_0 equal to about 1.6. Beyond the region of impact, as the boundary layer grows and the velocity at the outer edge of the boundary layer remains constant, friction decreases. Downstream of the convergence point, the friction continues to decrease. Within the hydraulic jump it takes a negative value, then again changes sign and after the jump it smoothly decreases with velocity.

Since the magnitude of the shear stress near the hydraulic jump is small, its measured results should be considered as appraising for the following reasons: first, as is shown in [17], with $\tau e^2/\mu D < 10^3$, there is deviation from relationship (44). Second, with shear stresses close to zero, the limiting diffusion current can be specified by the wall velocity expansion terms (in particular, by the quadratic term defined by the pressure gradient).

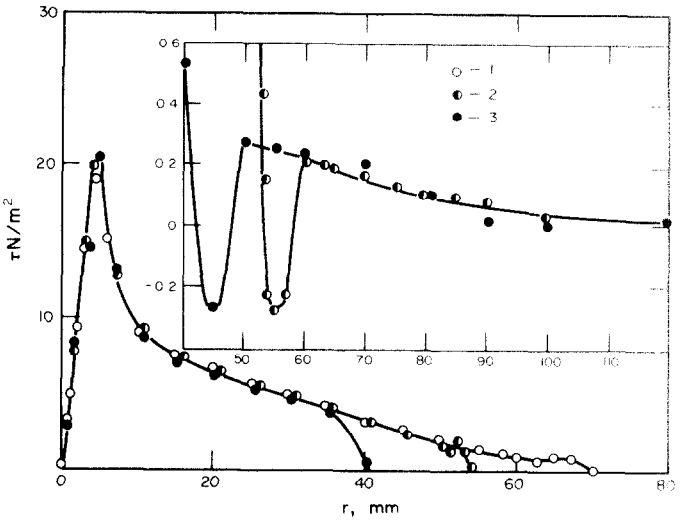

FIG. 2. Friction profile along the disk, $Q = 6.9 \times 10^{-5}$ m³/s: a, jump region; 1, rounded edge; 2, sharp edge; 3, $L = 1$ mm; 4, $L = 2$ mm.

Figure 2 also shows that the hydrodynamic conditions downstream of the jump have no effect on the upstream behavior, since the experimental data on the mean shear stress distribution prior to the jump coincide for all the conditions at the disk edge tested. Only a shift in the jump to the jet center is observed.

All the measured friction data prior to the jump are adequately correlated by the generalized coordinates $(\tau Q^2/\rho\nu^4; Q/\nu r)$, as is shown in Fig. 3. This figure also contains working formulas for all the flow regions.

The impingement zone friction data were used to calibrate the probes and are well described by curve I plotted according to Schlichting-Shach's formula (1a).

In the boundary-layer-type flow (II-2), the experimental data lie 8–10% below the results predicted by (12). This may be attributed to the hydrodynamic conditions in the impingement zone which are not taken into account in formula (12).

Within the region of "hydrodynamic stabilization", curve III corresponds to the asymptotic solution (15), while curve V, to the refined formula (14) for the laminar flow in the layer.

As is seen from the plot, with $Q/\nu r > 10^3$ the data obtained within the "stabilization" region are adequately described by curves IV and VI, which correspond to the asymptotic (20) and refined (19) solutions for the turbulent flow.

Thus, knowing the geometric and discharge parameters of the jet, one can readily calculate the friction in all the regions of the liquid layer wall flow.

4.3. *Friction pulsations*

Figure 4 illustrates a change in the relative dispersion of friction pulsations depending on $Q/\nu r$ for all the liquid flow rates studied. Here two maxima are clearly visible: one for the stagnation point and the other for the hydraulic jump. In the region of jet impingement, when $r = 2$ mm, the maximum level of pulsations ranges from 0.06 at $Q = 3.8 \times 10^{-5}$ m³/s to 0.315 at $Q = 2.24 \times 10^{-4}$ m³/s, while at the stagnation point the pulsation level increases sharply and can reach the values between 0.6–0.7.

In the II-2 region, the pulsation level does not exceed 0.08 for the majority of flow rates and for the maximum flow rate, $Q = 3.2 \times 10^{-4}$ m³/s, it does not exceed 0.18.

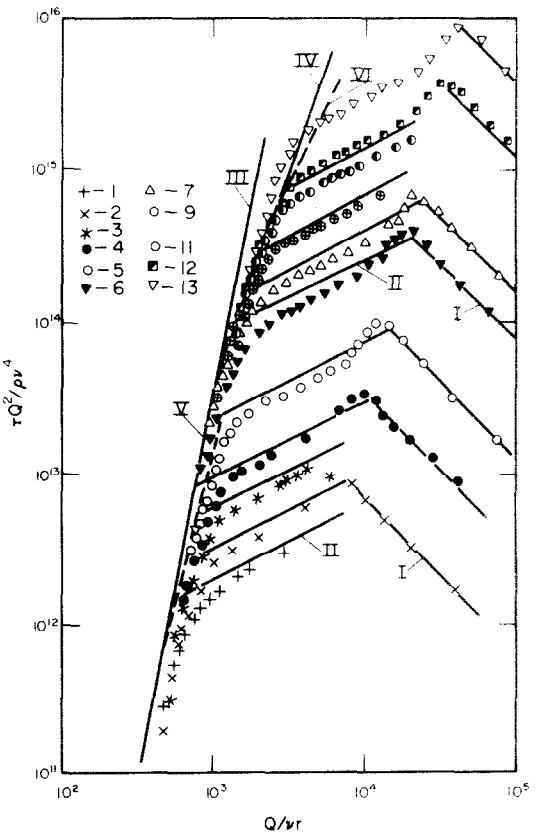

FIG. 3. Measured friction coefficients for all flow regions represented in generalized coordinates. Calculations: I, by (1a); II, by (12); III, by (15); IV, by (20); V, by (14); VI, by (19); Experiment: 1, $Q \times 10^5 = 1.36$ m³/s; 2, 1.88; 3, 2.64; 4, 3.8; 5, 6.9; 6, 12.1; 7, 14.0; 8, 15.7; 9, 17.3; 10, 18.3; 11, 22.4; 12, 24.3; 13, 32 m³/s.

This may be ascribed to the laminar flow regime in this region, which accords with the plot in Fig. 3.

In the II-4 region, the relative intensity of friction pulsations increases smoothly. Thus, for $Q = 1.4 \times 10^{-4}$ m^3/s, when $Q/\nu r = 1.2 \times 10^3$, the value of $(\overline{\tau'^2})^{1/2}/\tau$ is as high as 0.3. As seen from Fig. 4, for this very flow rate and the same magnitude of $Q/\nu r$, the measured mean friction data deviate from the laminar regime curve (III) and pass to the turbulent regime curve (IV). In the hydraulic jump region, the relative dispersion of friction pulsations reaches its maximum.

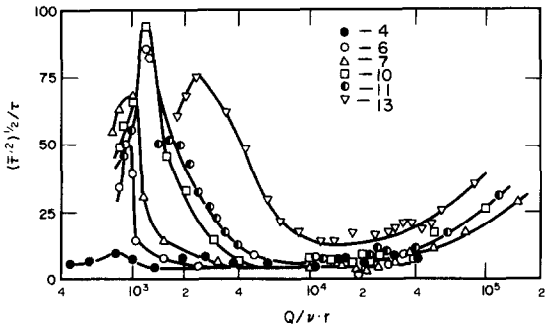

FIG. 4. Relative dispersion of friction pulsations vs $(Q/\nu r)$ for different liquid flow rates (see Fig. 3 for notation).

4.4. *Hydraulic jump*

To determine the hydraulic jump friction vector and its radius, the method of two probes was employed [14, 16]. This made it possible to reveal that in the jump region the friction takes a negative value, having changed sign twice, which points to liquid layer separation within the jump region. Besides, it allows the hydraulic jump radius and its radial width to be determined with high accuracy. As the jump radius r_1, that distance from the jet center was taken where the friction was minimal.

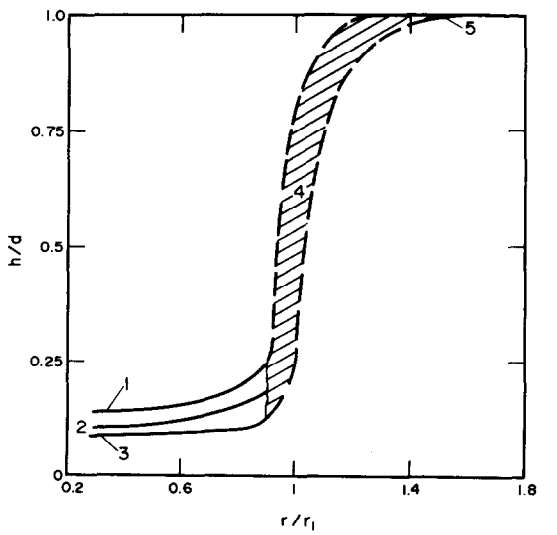

FIG. 5. Measured liquid layer thickness within the hydraulic jump given in dimensionless coordinates $(h/d; r/r_1)$: 1, sharp edge; 2, $L = 1$ mm; 3, $L = 2$ mm; 4, hydraulic jump; 5, layer thickness after the jump.

The simplest calculations of r_1 were made by Watson [1]. For a "jump", the condition of equality between the pressure discontinuity and the kinetic energy change is of the form

$$\frac{r_1 d^2 \cdot g \cdot r_0^2}{Q^2} + \frac{r_0^2}{2\pi^2 r_1 d} = \frac{2r_1 \cdot r_0^2}{Q^2} \int_0^h u^2 \cdot dz, \quad (47)$$

where d is the layer depth downstream of the jump.

The measured liquid film thickness within the jump is presented in Fig. 5 in the coordinates h/d and r/r_1 for all the flow rates and conditions at the disk edge tested. Here, the cross-hatched region represents the hydraulic jump where the accuracy of measurements was inadequate owing to the waves on the liquid surface. At $h = d$ this region passes into straight line 5. The plots show that the film thickness grows with approach to the jump and with increase in the drag at the disk edge. Far downstream of the jump the film thickness is constant.

Figure 6 represents experimental data of the present authors on the hydraulic jump radius for all the tested disk edge conditions given in the dimensionless coordinates $\bar{r}_1 = f(\bar{r})$ proposed by Watson, where

$$\bar{r}_1 = \lg[(r_1 d^2 \cdot g \cdot r_0^2/Q^2) + (r_0/2\pi^2 r_1 \cdot d)]$$
$$\bar{r} = \lg[(r_1/r_0)^3 (\nu r/Q)^{1/3}].$$

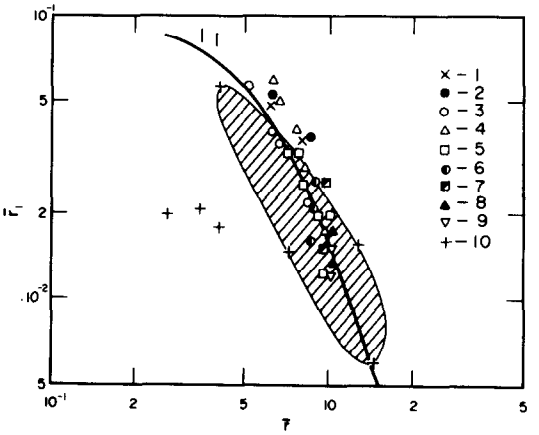

FIG. 6. Hydraulic jump radii for different liquid flow rates and disk edge conditions given in dimensionless coordinates: 1, $Q \times 10^5 = 1, 36$; 2, 3.8; 3, 6.9; 4, 14; 5, 18.8; 6, 22.4; 7, 24.3; 8, 28.3; 10, Watson's data; 11, calculation by (47).

Our experimental data are consistent with the theory of Watson, curve II. The plot also involves Watson's experimental data [1] on the hydraulic jump radius (the cross-hatched region and point 10).

Based on the "hydraulic" concepts about the jump origin, set forth for example in [18], the jump radius can be found from the condition $u = W$, where the liquid mass velocity, u, and the velocity of disturbance propagation over the shallow water surface, W, are calculated from

$$u = \frac{Q}{2\pi r h},$$
$$W = (gh)^{1/2}.$$

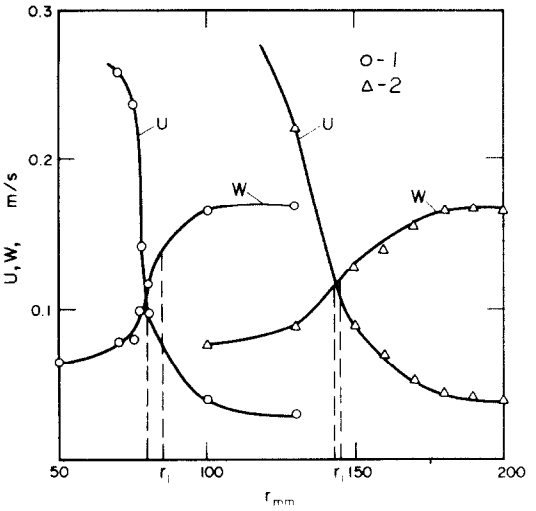

FIG. 7. Jump radii based on the liquid flow rate and the shallow water surface disturbance rate: 1, $Q = 6.9 \times 10^{-5}$ m^3/s; 2, 14×10^{-5} m^3/s.

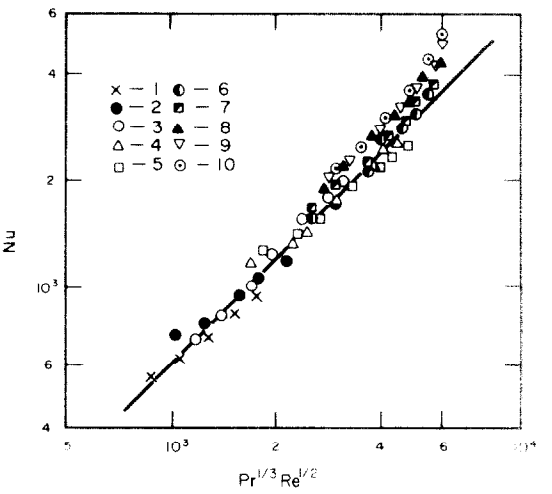

FIG. 9. Mass transfer in the region of the boundary-layer-type flow: 1, $Q = 6.9 \times 10^{-5}$ m^3/s; 2, 3.8; 3, 6.9; 4, 14; 5, 18.8; 6, 22.4; 7, 24.3; 8, 28.3; 9, 32; 10, 37.2; I, calculation by (31).

Comparison of these velocities for two liquid flow rates is given in Fig. 7. It may be seen there that the jump radius, which is defined from the condition $u = W$, is about the same as that which is found by the electrodiffusion method. It is of great interest to study, both theoretically and experimentally, the flow region downstream of the jump.

4.5. *Mass-transfer measurements*

The local mass-transfer coefficient along the disk radius was measured for all the flow regions in the range of the jet liquid flow rates from 1.36×10^{-5} to 3.2×10^{-4} m^3/s. The results for one value of the liquid flow rate are given in Fig. 8 as a function of r for all the disk edge conditions tested. The analysis of these data shows that the trend in the dependence of β on r, the liquid flow rate and on the disk edge conditions is analogous to that revealed by the measured friction data. Thus, the maximum value of β corresponds to $r/r_0 \approx 1.6$. As r grows, the mass-transfer coefficient falls to the values which are minimal in the hydraulic jump region. It should be noted that the local mass-transfer coefficient exhibits the same qualitative behavior in the zone of impact and in the region of the submerged jet boundary-layer-type flow [9]. However, as shown in [9], the method of transcinnamic acid dissolution can lead to a significant increase in mass transfer within the impingement zone due to wall erosion.

In the region downstream of the jump, β first increases (Fig. 8) and then decreases smoothly. However, starting from some liquid flow rates (e.g. $Q = 1.4 \times 10^{-4}$ m^3/s) in the region of "hydrodynamic stabilization", the mass-transfer coefficient, in contrast to friction, increases substantially. Special measurements of β, with a surfactant added into the electrolyte.

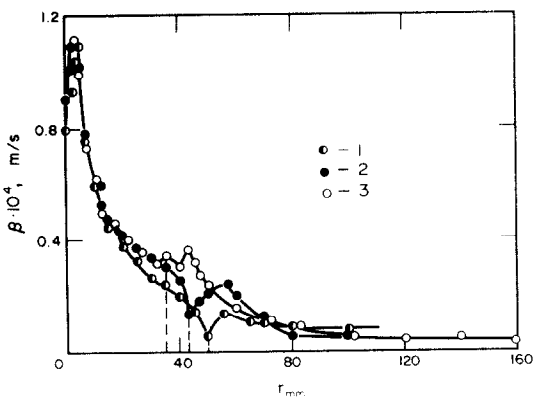

FIG. 8. Local mass-transfer coefficients along the disk for different disk edge conditions: $Q = 6.9 \times 10^{-5}$ m^3/s; 1, sharp edge; 2, $L = 1$ mm; 3, $L = 3$ mm.

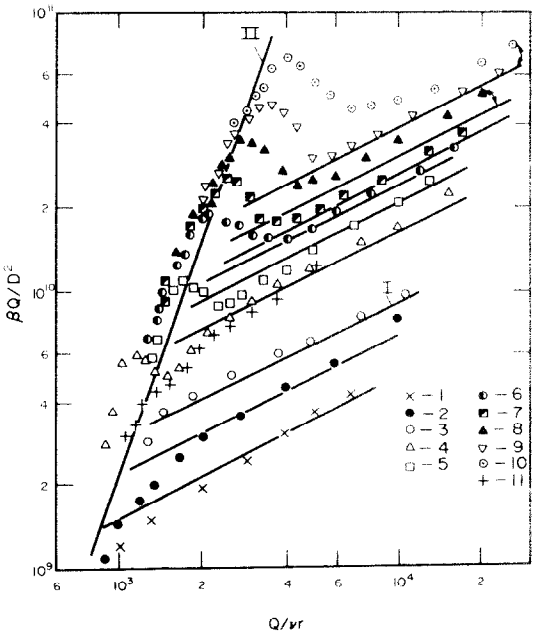

FIG. 10. Experimental results on mass transfer for all the flow regions represented in generalized coordinates. 1–10 (see Fig. 9 for notation); 2, with addition of surfactant. Calculation: I, by (32); II, by (42).

as well as observation of the liquid film surface with stroboscopic illumination allow the conclusion that an increase in β may be attributed to formation of waves on the film surface in this region. It should be noted that all the physical constants of the electrolyte remain unchanged except for the surface tension coefficient. In the case of a pure electrolyte $\sigma = 7.05 \times 10^{-2}$ N/m, while with a foaming agent $\sigma = 3.24 \times 10^{-2}$ N/m.

The experimental data on the boundary-layer-type flow are well described by relationship (31) for all the investigated liquid flow rates (Fig. 9). Deviation from the predicted values at $Pr^{1/3} \cdot Re^{1/2} > 5$ corresponds to the onset of transition to the "stabilized" (steady-state) flow.

All the measured mass-transfer coefficients are adequately correlated in the coordinates ($\beta Q/D^2$ and Q/vr), as shown in Fig. 10. Here are also presented the results of calculations of the boundary-layer-type flow (curve I) by formula (31) and of the flow downstream of the convergence point (curve II) by asymptotic formula (42). As seen, without film surface waves (points-II) formula (42) fits the experimental data well.

Thus, knowing the nozzle geometry, the flow rate and physical characteristics of the working fluid, the local mass-transfer coefficients may be readily calculated by formulae (31) and (42) within the entire laminar flow region of the horizontal wall radial jet.

REFERENCES

1. E. J. Watson, The radial spread of a liquid jet over a horizontal plane, *J. Fluid Mech.* **20**, 481–499 (1964).
2. H. Schlichting, *Boundary Layer Theory*. McGraw-Hill, New York (1960).
3. W. Shach, Umlenkung eines kreisförmigen Flussigkeitsstrahles an einer ebenen Platte senkrecht zur Strömungsrichtung, *Ing.-Arch.* **1**, 51–59 (1935).
4. M. B. Glauert, The wall jet, *J. Fluid Mech.* **1**, 625–637 (1956).
5. Z. H. Chaudhury, Heat transfer in a radial liquid jet, *J. Fluid Mech.* **20**, 501–511 (1964).
6. W. Shach, Umlenkung eines Flussigkeitsstrahles an einer ebenen Platte, *Ing.-Arch.* **5**(4), 245–265 (1934).
7. G. Grigoryan, Some dynamic aspects of non-submerged liquid jets impinging onto a solid surface, *Trudy Azerb. Nauchn.-Issled. Inst. Mekh. Elektrofik. Selskogo Khoz.* **1**, 7–15 (1963).
8. R. G. Olsson, Radial spread of a liquid stream on a horizontal plate, *Nature* **211**(5051), 813–816 (1966).
9. V. V. Rao and T. Olev, Mass transfer from a flat surface to an impinging turbulent jet, *Can. J. Chem. Engng* **42**(3), 95–99 (1964).
10. D. C. McMurray, P. S. Myers and O. A. Uyehers, Influence of impinging jet variables on local heat-transfer coefficient along a flat surface with constant heat flux, in *3rd International Heat Transfer Conference, Chicago*, Vol. 2, pp. 292–298 (1966).
11. L. G. Loitsyanskii, *Laminar Boundary Layer*. Fizmatgiz, Moscow (1962).
12. S. S. Kutateladze (Editor), *Wave Processes in Two-Phase Systems, Collected Papers*. Inst. of Thermophysics, Novosibirsk (1975).
13. V. G. Levich, *Physicochemical Hydrodynamics*. Fizmatgiz, Moscow (1959).
14. A. J. Karabelas and T. J. Hamtty, Determination of surface velocity gradient in three-dimensional boundary layer, *J. Fluid Mech.* **34**, 159–162 (1968).
15. S. S. Kutateladze, V. E. Nakoryakov, A. P. Burdukov and V. A. Kuzmin, Application of electrochemical method to measuring friction in two-phase media hydrodynamics, in *Collected Papers Heat and Mass Transfer*, Vol. 2. Minsk (1968).
16. S. S. Kutateladze (Editor), *Turbulent Flows in Two-Phase Media, Collected Papers*. ITP, Novosibirsk (1973).
17. J. Cognet, Utilisation de la polarographie pour l'etude de l'ecoulement de Couette, *J. Mec.* **10**(1), 65–90 (1971).
18. L. D. Landau and E. M. Lifshits, *The Mechanics of Continuous Media*. GITTL, Moscow (1954).

IMPACT D'UN JET LIQUIDE AXISYMETRIQUE SUR UNE BARRIERE

Résumé—Dans quelques technologies métallurgiques et chimiques l'utilisation de jets liquides frappant une paroi est un moyen efficace d'accroitre le transfert massique ou thermique. Le but de cet article est d'étudier à la fois théoriquement et expérimentalement l'hydrodynamique et le transfert massique d'un jet liquide circulaire frappant un plan horizontal. Le champ de l'écoulement, du point d'arrêt au saut hydraulique, est décrit dans le cadre des approximations de la théorie de la couche limite pour les régimes laminaire et turbulent dans une mince couche liquide. On a obtenu des formules simples pour le calcul du frottement, de l'épaisseur de la couche liquide et de la vitesse à la surface du liquide en fonction des paramètres à la tuyère. Une solution est proposée pour le problème du transfert massique à la paroi pour la région laminaire avant le saut et on a obtenu des formules pratiques pour le calcul du coefficient du transfert massique. Les tensions pariétales, les coefficients locaux et moyens de transfert massique dans la région d'écoulement ont été mesurés par une méthode d'électrodiffusion, dans un large domaine de débits et de conditions pour lesquelles l'écoulement quitte la barrière. On a étudié aussi les caractéristiques hydrodynamiques du jet autour du point d'impact et du saut hydraulique. Les résultats expérimentaux sont donnés en fonction des coordonnées généralisées et comparés avec les équations théoriques appropriées.

DAS AUFPRALLEN EINES ACHSENSYMMETRISCHEN STRAHLES AUF EINEN STAUKÖRPER

Zusammenfassung—Für einige technologische Anwendungen der Metallurgie und der technischen Chemie erscheint das Aufprallen eines zähen Flüssigkeitsstrahls auf eine Wand als wirksames Mittel zur Verbesserung von Wärme- und Stoffübertragungsvorgängen. Ziel der voliegenden Arbeit war die theoretische und experimentelle Untersuchung von Hydrodynamik und Stofftransport in einem radial

gerichteten Flüssigkeitsstrom nach Auftreffen auf eine horizontale Fläche. Das gesamte Strömungsfeld vom Staupunkt bis zum Wassersprung—wird im Rahmen der Vernachlässigungen der Grenzschichttheorie sowohl für den laminaren als auch für den turbulenten Bereich einer dünnen Strömungsschicht beschrieben. Man erhält einfache Formeln zur Berechnung des Reibungsfaktors, der Grenzschichtdicke und der Oberflächengeschwindigkeit der Flüssigkeit als Funktion der Strömungsparameter. Für das Problem des Stofftransports von der Wand an eine Flüssigkeitsschicht wird eine Lösung angeboten, gültig für das gesamte laminare Strömungsgebiet vor dem Wassersprung. Man erhält einfache Arbeitsformeln zur Berechnung des Stofftransportkoeffizienten. Die Wandschubspannung und die lokalen und globalen Stoffübergangskoeffizienten im gesamten Strömungsgebiet wurden mit Hilfe einer Elektrodiffusionsmethode gemessen, und zwar für einen weiten Bereich von Massenströmen und Abströmbedingungen vom Staukörper. Ebenso wurden die hydrodynamischen Eigenschaften des Strahls am Aufprallpunkt und beim Wassersprung untersucht. Die Versuchsergebnisse werden in normierten Koordinaten mitgeteilt und mit geeigneten theoretischen Beziehungen verglichen.

НАБЕГАНИЕ ОСЕСИММЕТРИЧНОЙ СТРУИ ЖИДКОСТИ НА ПРЕГРАДУ

Аннотация — В ряде технологий металлургической и химической промышленностей повышение эффективности процессов тепло- и массопереноса достигается использованием струй тяжелой жидкости, падающих на стенку. Цель настоящей статьи — теоретическое и экспериментальное исследование гидродинамики и массообмена радиальной струи жидкости, набегающей на горизонтальную плиту. В рамках приближений теории пограничного слоя описано все поле течения от критической точки вплоть до гидравлического скачка, как для ламинарного так и турбулентного режимов течения в тонком слое жидкости. Получены простые формулы для расчета коэффициента трения, толщины слоя жидкости, скорости жидкости на поверхности в зависимости от расходных параметров. Решена задача массоотдачи от стенки к слою жидкости для всей области течения вплоть до скачка в случае ламинарного режима течения и получены простые расчетные формулы для коэффициентов массоотдачи. Используя электродиффузионный метод, измерены касательные напряжения трения на стенке, локальные и средние коэффициенты массоотдачи во всей области течения жидкости в широком диапазоне изменения расходов жидкости и условий слива жидкости с преграды. Исследованы также гидродинамические характеристики струи в месте удара и гадравлического скачка. Результаты экспериментов представлены в обобщенных координатах и сопоставлены с соответствующими расчетными формулами.